Peptide Materials Obtained by Aggregation of Polyphenylalanine Conjugates as Gadolinium-Based Magnetic Resonance Imaging Contrast Agents

*Carlo Diaferia, Eliana Gianolio, Pasquale Palladino, Francesca Arena, Cinzia Boffa, Giancarlo Morelli, and Antonella Accardo**

Peptide materials based on the aggregation of polyphenylalanine conjugates containing gadolinium complexes and acting as potential contrast agents (CAs) in magnetic resonance imaging (MRI) are described. Monomers contain two (F2) or four (F4) phenylalanine residues for self-assembly, a chelating agent, 1,4,7,10-tetraazacyclododecane-*N*,*N*,*N*,*N*-tetraacetic acid (DOTA) or diethylenetriaminepentaacetic acid (DTPA), for achieving gadolinium coordination, and ethoxylic linkers at two (L_2) or six (L_6) poly(ethylene glycol) (PEG) units between the chelating group and the peptide region. Both DOTA and DTPA tetraphenylalanine derivatives, and their gadolinium complexes DOTA(Gd)-L_6-F4 and DTPA(Gd)-L_6-F4, are able to self-aggregate at very low concentration. Structural characterization, obtained by circular dichroism and infrared measurements, confirms the amyloid type fibril formation in which an antiparallel peptide alignment is preferred. Amyloid type fibril formation is also observed, in solid state, by transmission electron microscopy images and X-ray diffraction patterns. The relaxivity values of DOTA(Gd)-L_6-F4 and DTPA(Gd)-L_6-F4 and their ability to enhance the MRI cellular response on the J774A.1 mouse macrophages cell line indicate that these peptide materials are promising candidate as a new class of supramolecular gadolinium based MRI contrast agents.

1. Introduction

In the last few years an explosion of interest has been focused on the design, synthesis, and characterization of peptide-based materials for nanomedicine and nanoscience.[1–3] The advancement of knowledge about molecular mechanism and forces that determine the growth of nanometric structures from basic peptide motifs from one side, and the applicative outcome in the obtainment of peptide-based nanodevices for electronics, biosensing, coating for tissue engineering and cell adhesion, and drug delivery from the other side, have rapidly reached successful results.[4]

This has been achieved by mimicking the strategies that nature pursues in the construction of complex supramolecular aggregates, essentially based on self-assembly and bottom-up procedures.

A large number of peptide-based building blocks, comprising cyclic peptides, amphiphile peptides, dendritic peptides, and aromatic dipeptides, have been considered for generating self-assembled nanostructures.[5–8]

Among the different applications of peptide-based materials, there are several advantages, such as the intrinsic biological origin, low immunogenicity, biocompatibility, low cost, high stability, ability for specific molecular recognition, long-term storage, and easy handling, that make synthetic peptides useful and versatile building blocks for applications in biomedical field.

The self-aggregation of short peptide sequences can be catalysed by the insertion of nonpeptidic hydrophobic groups, such as aliphatic chains[9,10] or cholesterol derivatives,[11] or introducing amino acids able to promote aromatic π-stacking interactions between their side chains, such as phenylalanine, tyrosine, and tryptophan.[6]

Intense stimulus in this research area was promoted by the identification of some natural self-aggregation patterns, such as diphenylalanine (FF) motive. Diphenylalanine, which constitutes the core recognition motif of Alzheimer's β-amyloid peptide, is able to self-assemble into many different nanostructures from nanotubes to organogels.[12,13]

FF nanostructures have been investigated for their mechanical, electrochemical, and optical properties. Many studies reported in literature are principally focused on clarifying the physicochemical aspects responsible for array stability in FF nanostructures,[14–16] whereas only few studies have been devoted in the investigation of FF aggregates for biomedical

Dr. C. Diaferia, Prof. G. Morelli, Dr. A. Accardo
Department of Pharmacy
Research Centre on Bioactive Peptides (CIRPeB)
University of Naples "Federico II" and DFM Scarl
Via Mezzocannone 16, 80134 Naples, Italy
E-mail: antonella.accardo@unina.it
Dr. E. Gianolio, Dr. F. Arena, Dr. C. Boffa
Department of Molecular Biotechnologies and Health Science
University of Turin
Via Nizza 52, 10125 Turin, Italy
Dr. P. Palladino
Department of Chemical Sciences
University of Catania
Viale A. Doria 6, 95124 Catania, Italy
Dr. P. Palladino
I. N. B. B. Consortium
Viale delle Medaglie D'Oro 305, 00136 Rome, Italy

DOI: 10.1002/adfm.201502458

applications,[17–19] essentially due to their intrinsic low water solubility.[20]

Very recently two examples of cationic diphenylalanine based microtubes (FF-MTs) and nanoparticles (CDPNCs) have been reported as potential vehicles for drug delivery.[21,22] However, research on FF-based compounds as diagnostic tools remains largely unexplored. Here, we describe new peptide materials based on poly-phenylalanine conjugates as potential contrast agents in magnetic resonance imaging (MRI).

The paramagnetic gadolinium complexes currently used in clinical diagnosis as MRI contrast agents are essentially low molecular weight compounds that rapidly equilibrate between the intra- and extravascular spaces after intravenous administration. However, gadolinium-based supramolecular aggregates, such as micelles,[23,24] liposomes,[25,26] and peptide amphiphile nanofibers[27,28] have been proposed as MRI contrast agents in order to obtain enhanced contrast efficacy and different pharmacokinetic behavior.[29,30] It is known, in fact, that the ability of a MRI contrast agent to act as water proton relaxation agent is proportional to its molecular weight.[29,30]

Here we report the aggregation properties of phenylalanine derivatives displayed in **Figure 1**A, together with their relaxometric behavior, cytotoxicity, and cellular uptake in J774A.1 and 3T3 cells.

2. Results and Discussion

2.1. Design, Synthesis, and Aggregation Behavior

Various aromatic amino acids (phenylalanine, tryptophan, and tyrosine) and other aromatic moieties (naphthalene, azobenzene, and pyrene) have been proposed as building block for the synthesis of new nanomaterials. The structural properties of the resulting materials strongly depend from several parameters including hydrophilicity/hydrophobicity and extent of the aromatic ring. The self-asembling peptide derivatives here proposed as MRI contrast agents are based on poly-phenylalanine conjugates. Poly-phenylalanine conjugates, schematically represented in Figure 1A, contain two (F2) or four (F4) phenylalanine residues for self-assembly, a bifunctional chelating agent, 1,4,7,10-tetraazacyclododecane-*N,N,N,N*-tetraacetic acid (DOTA) or diethylenetriaminepentaacetic acid (DTPA), for achieving gadolinium coordination and an ethoxylic linker consisting of two (L_2) or six (L_6) PEG units between the chelating group and peptide region. All compounds were obtained by Fmoc/tBu solid phase synthesis in good yield and high purity. The relative simple self-organization of di-phenylalanine depends on a combination of two kinds of not covalent interactions: i) head-to-tail backbone hydrogen bonds and ii) π–π stacking between the aromatic ring of side chains.[14] Hydrogen bonds and π–π stacking are weak not covalent interactions that occur only if mutual guidance and directionality of the counterparts are kept. As a consequence, any modification of the peptide requires a careful design. First of all, it is well known that chemical modifications of Phe–Phe homo-dimer at C or N-terminus may destroy the head-to-tail intermolecular hydrogen bonds, whereas π–π intermolecular interaction of the aromatic framework should be kept. However, independently from the chelating agent used, di-phenylalanine conjugates DOTA(Gd)-F2 and DTPA(Gd)-F2 here reported do not show propensity to aggregate in water solution (data not shown), probably due to the steric hindrance of the bulk gadolinium complex, even with the insertion of L_2 ethoxylic spacer between the peptide framework and the chelating agent.

Differently, UV–vis and fluorescence measurements suggest a weak aggregation tendency for DOTA-L_6-F2 and DTPA-L_6-F2 conjugates, in which L_2 spacer is replaced with L_6 spacer at six ethoxylic units (Figure 1A). UV–vis spectra show the typical maximum of Phe residue at 257 nm (n $\rightarrow$ π transition of the aromatic residue), and another maximum at 282 nm, distinctive of the Phe excimer formation (data not shown).[31] Accordingly,

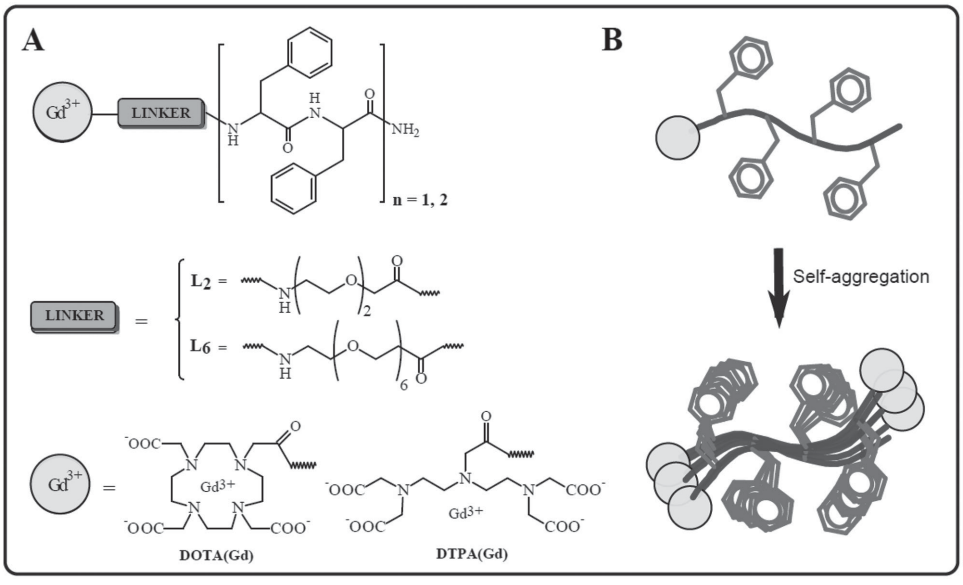

Figure 1. A) Schematic representation of diphenylalanine or tetraphenylalanine conjugates, obtained using L_2 or L_6 polyethoxylic linkers and the DTPA(Gd) or DOTA(Gd) gadolinium complexes. B) Putative aggregation pattern for polyphenylalanine conjugates.

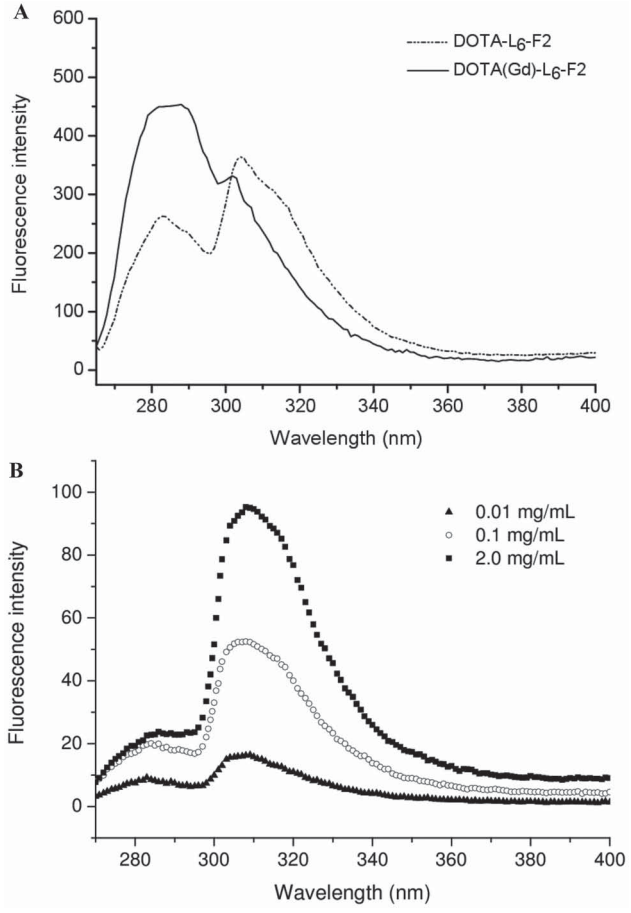

Figure 2. Fluorescence spectra of A) DOTA-L_6-F2 and its gadolinium complex DOTA(Gd)-L_6-F2 in water solution at 2.0 mg mL^{-1} and B) DOTA(Gd)-L_6-F4 tetra-phenylalanine at a concentration of 0.01, 0.1, and 2.0 mg mL^{-1}. All emission spectra were recorded at 25 °C between 265 and 400 nm with excitation at 258 nm.

fluorescence spectrum of DOTA-L_6-F2 at 2.0 mg mL^{-1} reported in **Figure 2**A clearly shows the monomer emission at 282 nm and the conspicuous excimer emission around 310 nm.[32] However, the emission peak of phenylalanine excimer almost disappears after the gadolinium complexation (see Figure 2A).

The same behavior is also displayed by DTPA-L_6-F2. This outcome could be attributed to the higher steric effect of gadolinium complex with respect to the chelating agent as free base. In order to restore the interactions between the phenylalanine side chains, the peptide framework was reinforced by increasing the number of the phenylalanine residues from two to four, keeping unaltered the length of the spacer. These optimized conjugates DOTA(Gd)-L_6-F4 and DTPA(Gd)-L_6-F4 show high water solubility: their solutions appear perfectly clear up to 35 mg mL^{-1}; whereas higher concentration (50 mg mL^{-1}) leads to a hydrogel formation. The same behavior is also observed for L_6-F4 derivative lacking of chelating agent at the N-terminus. Fluorescence spectra of DOTA(Gd)-L_6-F4 at three different concentrations (0.01, 0.1, and 2.0 mg mL^{-1}) reported in Figure 2B show both the Phe (λ_{282}) and its excimer (λ_{310}) emission peaks, thus confirming the high propensity of the complex to aggregate, also at low concentration. Furthermore, by increasing the concentration of DOTA(Gd)-L_6-F4 from 0.01 to 2.0 mg mL^{-1}, a progressive increase (from 1.7 to 4.0) of the ratio between the fluorescence intensities at λ_{310} and λ_{282} is observed. The potential of nanosized supramolecular systems in the field of drug delivery and diagnostic biomedical applications has been investigated from many years. In particular, if MRI diagnostic systems are considered, the possibility to exploit large-sized macromolecules is favourable also from the contrast efficiency point of view. For this reason, on the basis of the preliminary aggregation data, the Gd-complexes of the tetra-phenylalanine conjugates, endowed with the highest propensity to aggregation, were selected to be further investigated for a relaxometric and structural characterization. Moreover, their cytotoxicity and cellular uptake capacity were investigated in J774A.1 and 3T3 cell lines.

2.2. Fluorescence Spectroscopy

Critical aggregate concentration (CAC) values of tetraphenylalanine derivatives as free basis or as gadolinium complexes were quantitatively estimated with a fluorescence-based method using 8-anilinonaphthalene-1-sulfonate (ANS) as probe. ANS fluorophore gives fluorescence emission at 460–480 nm only in a hydrophobic environment, such as in the micelle core.[33] The fluorescence intensity of an ANS solutions (20×10^{-6} M in water) at 475 nm as function of tetra-phenylalanine derivatives concentration are reported in **Figure 3**, and the CAC values of the aggregates were determined at the break point (**Table 1**). During the titration experiment, the fluorescence emission of DOTA-L_6-F4 remains unchanged until 75×10^{-6} M (≈0.099 mg mL^{-1}), whereas an increase in the signal at 475 nm was detected above this concentration value, indicating the self-organization of the tetraphenylalanine derivative (Figure 3A). Usually, in the molecules containing chelating agents, aggregation properties can be influenced by two different phenomena: electrostatic repulsions and/or steric hindrance.[29] However, only a slight decrease in the CAC value is observed after the gadolinium complexation that reduces the negative charge from −3 to 0 (CAC = 0.076 mg mL^{-1} for DOTA(Gd)-L_6-F4). On the contrary, a significant change has been observed when DOTA is replaced by the branched chelator DTPA (CAC = 0.59 mg mL^{-1}) or by its gadolinium complex DTPA(Gd) (CAC = 0.51 mg mL^{-1}) (see Figure 3B and Table 1). These results suggest that the influence of electrostatic repulsions is almost negligible, whereas the replacement of the macrocycle DOTA with the branched and bulky DTPA produces an increase of the CAC values.

Aggregation of tetraphenylalanine derivatives was also investigated by monitoring fluorescence behavior of pyrene (Pyr). 1×10^{-6} M Pyr solution was titrated by adding increasing amounts of tetraphenylalanine derivatives. Fluorescence spectra of Pyr/DOTA(Gd)-L_6-F4 solutions are reported in **Figure 4**A,B. Pyr is a poorly soluble water molecule that shows an emission spectrum in water with five vibrational bands when excited at λ = 335 nm: the first (I_1 at 373 nm) and the third (I_3 at 383 nm) of them are strongly affected by the polarity of the surrounding environment. Moreover, at high concentration Pyr gives stacking phenomena resulting in excimer's formation that can be diagnosed by the appearance of a maximum at around 480 nm.[10]

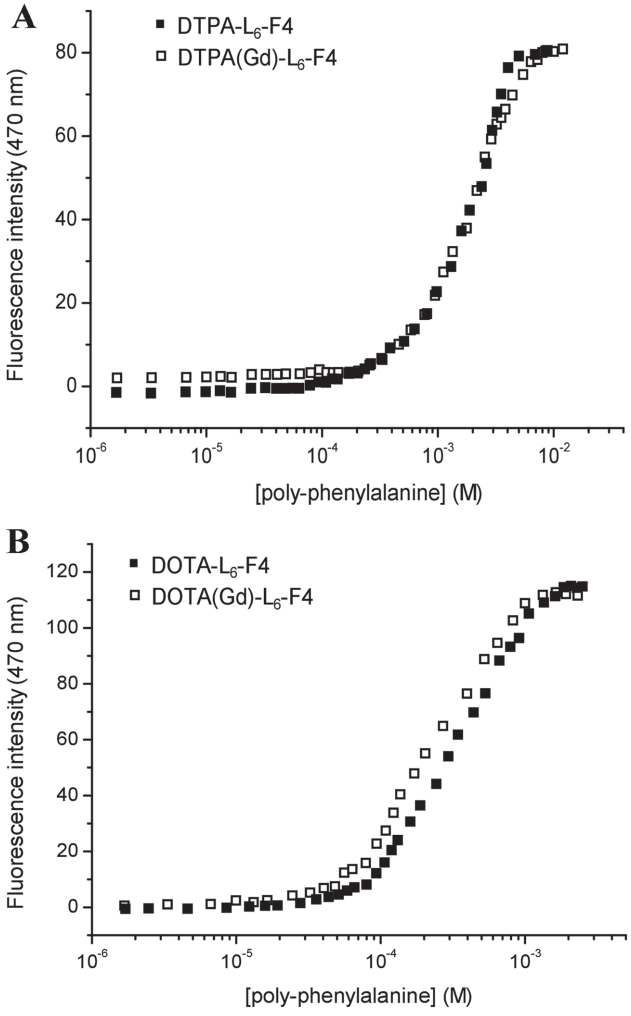

Figure 3. Fluorescence intensity emission of the ANS fluorophore at 475 nm versus the concentration of A) DTPA-L_6-F4 and B) DOTA-L_6-F4 as free bases or as gadolinium complexes. CAC values are established from the break points.

The addition of small amounts of DOTA(Gd)-L_6-F4 to Pyr solution causes a progressive decrease of fluorescence signal (Figure 4A). This effect was observed until concentration 14.3×10^{-6} M of tetra-phenylalanine derivative, in which Pyr/DOTA(Gd)-L_6-F4 molar ratio is 1/10. On the contrary, at concentration of 167×10^{-6} M and higher, an increase of the fluorescence intensities occurs. These data indicate that the aggregation phenomenon occurs at concentration within the 14.3×10^{-6} M to 167×10^{-6} M range, in agreement with the CAC value (51×10^{-6} M) found by ANS titration, suggesting that when DOTA(Gd)-L_6-F4 concentration is lower than 14.3×10^{-6} M, the predominant effect is a quenching due to the aromatic stacking between phenylalanine residues and pyrene, whereas above this concentration, a fluorescence resonance energy transfer (FRET) effect occurs in which tetra-phenylalanines, in their aggregated form, act as donor for pyrene.

Table 1. Critical aggregate concentration (CAC) values of tetraphenylalanine derivatives measured by titration of the ANS fluorophore.

Sample	CAC [M]	CAC [mg mL^{-1}]
DOTA-L_6-F4	7.5×10^{-5}	9.9×10^{-2}
DOTA(Gd)-L_6-F4	5.1×10^{-5}	7.6×10^{-2}
DTPA-L_6-F4	4.5×10^{-4}	59×10^{-2}
DTPA(Gd)-L_6-F4	3.5×10^{-4}	51×10^{-2}

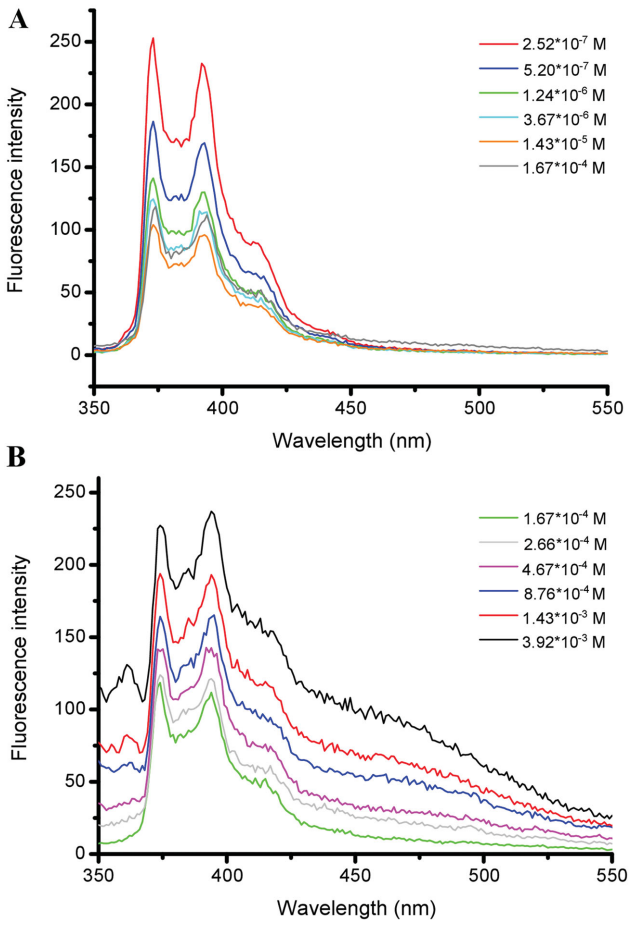

Figure 4. Fluorescence spectra of a 1×10^{-6} M pyrene solution titrated with DOTA(Gd)-L_6-F4. Pyr emission spectra were recorded at 25 °C between 350 and 550 nm with excitation at 335 nm.

2.3. Secondary Structure

The secondary structure of DOTA-L_6-F4 and DTPA-L_6-F4 peptide derivatives, as free bases or as gadolinium complexes, was assessed using circular dichroism (CD in **Figure 5** and Figures S1–S5, Supporting Information) and Fourier transform infrared spectroscopies (FTIR in **Figure 6**A).

CD spectra of solutions at several concentrations were recorded between 280 and 195 nm. CD spectra at concentrations below or close to CAC values clearly show two maxima around 205 and 220 nm, due to aromatic side-chains stacking, and pronounced minimum at 232 nm, which can be associated with a β-structure.[31,34] Significant conformational transition was observed at higher concentrations, where the

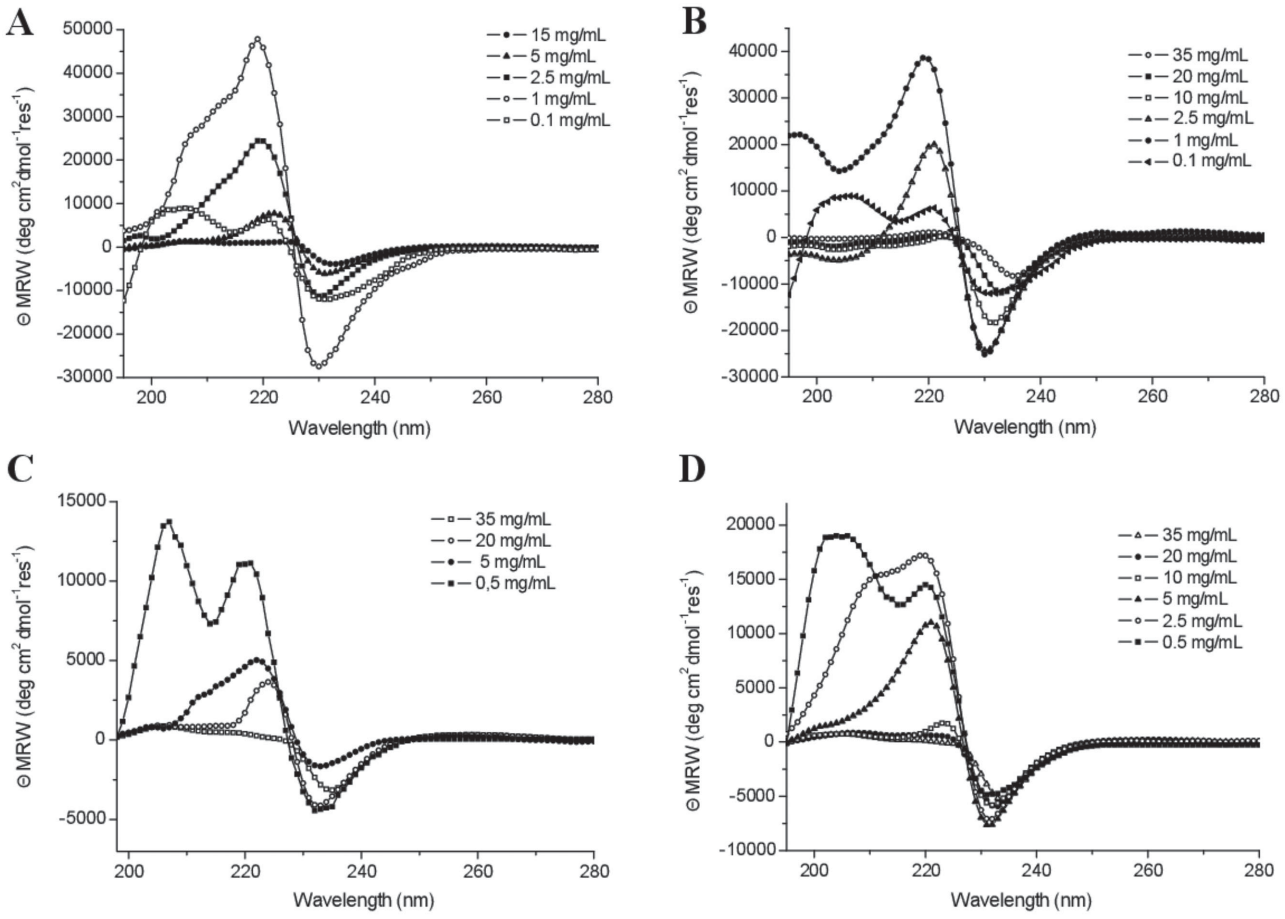

Figure 5. Selected Far-UV CD spectra of A) DOTA-L_6-F4, B) DOTA(Gd)-L_6-F4, C) DTPA-L_6-F4, and D) DTPA(Gd)-L_6-F4 in a concentration range of 0.1–35 mg mL^{-1}.

main minimum at 230 nm and the absence of the maxima above reported can be interpreted as a signature for the dominant β-sheet arrangements.[31,34] From the inspection of Figure 5, the CD spectra of peptide derivatives show similar trend irrespective of chelating agent. However, the conformational transition described above was detected at higher concentration for DTPA-L_6-F4 than DOTA-L_6-F4, in agreement with the difference in CAC values between these conjugates. Dichroic tendency of DOTA(Gd)-L_6-F4 at 20 mg mL^{-1} (well above the CAC value determined by fluorescence) was also evaluated as function of the temperature between 10 and 80 °C. At low temperature, it was observed a distinct minimum around 235 nm, typical of the polyphenylalanine in β-aggregate form (Figure S5A, Supporting Information). By increasing the temperature, the shape of the spectra remains unchanged, but a progressive decrease of the signal intensities with a red-shift effect occurs probably due to a progressive unfolding of the peptide conjugate with higher molecular mobility. However, the conformational features are kept almost until 80 °C, thus indicating a good thermal stability of the aggregate.[35] The integrity of the gadolinium complex in DOTA(Gd)-L_6-F4 at the final temperature (80 °C) was confirmed by the mass peak reported in Figure S5B of the Supporting Information.

IR spectroscopy is often employed to probe the secondary structure assumed by di- or tetraphenylalanine derivatives.[17,36] Usually, the attention is focused on the amide I bands able to provide information on the secondary structure adopted. FTIR spectra in the amide I region are shown in Figure 6A for DTPA(Gd)-L_6-F4 and DOTA(Gd)-L_6-F4 solutions at 2.0 mg mL^{-1}. Both the spectra show a principal peak at 1637 cm^{-1} and a minor peak at 1680 cm^{-1}. The peak at 1637 cm^{-1} is strongly indicative of β-sheet formation, whereas the fewer intensity of the second peak at 1680 cm^{-1} is indicative of an antiparallel orientation of the β-sheets.[37] FTIR spectra were also recorded on a dried film of DTPA(Gd)-L_6-F4 and DOTA(Gd)-L_6-F4 (see Figure S6, Supporting Information). These spectra reported a similar profile with respect to samples in solution.

Amyloid type fibril formation was also confirmed by using the typical Thioflavin T and Congo Red spectroscopic assays. Fluorescence spectra of ThT, before and after the addition of DOTA-L_6-F4, are reported in Figure S7 of the Supporting Information. Spectra of DOTA-L_6-F4 and its gadolinium complex in absence of ThT are also reported for comparison.

As shown in Figure S7 of the Supporting Information, DOTA(Gd)-L_6-F4 gadolinium complex alone gives an emission peak in the same region in which the emission of ThT-β aggregate is expected.

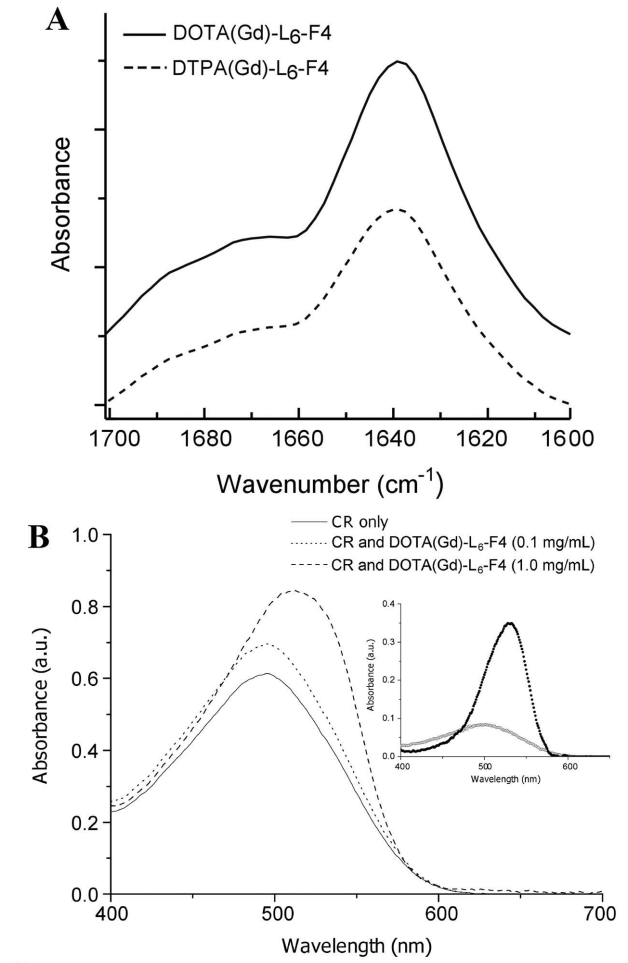

Figure 6. A) FTIR spectra of DOTA(Gd)-L_6-F4 and DTPA(Gd)-L_6-F4 in the amide I region at 2.0 mg mL^{-1} concentration. B) The UV–vis spectra of DOTA(Gd)-L_6-F4, stained with Congo Red, at 0.1 and 1.0 mg mL^{-1}. The spectrum of Congo Red is also reported for comparison. Insets: The spectra of DOTA(Gd)-L_6-F4 0.1 mg (○) and 1.0 mg mL^{-1} (●) after the subtraction of the CR spectrum. C) Polarized optical microscopy image of dried DOTA(Gd)-L_6-F4 on a glass microscopy slide stained with Congo Red solution.

As a consequence, in this sample we cannot attribute the peak at 482 nm to the interaction between ThT and the tetra-phenylalanine aggregate. On the contrary, in its uncomplexed form, DOTA chelating agent did not provide fluorescence signals. The sudden appearance of an emission peak at 482 nm after the addition of DOTA-L_6-F4 (2.0 mg mL^{-1} as final concentration) indicates unambiguously the binding of the ThT to the peptide derivatives.[38] The fluorescence signal remains unchanged until 2 h from the incubation, thus confirming the immediate interaction of ThT with peptides. The same behavior was also observed for tetra-phenylalanine analogues containing DTPA chelating agent and its gadolinium complex (data not shown). According to the ThT assay, Congo Red staining (both UV–vis spectroscopy and polarized optical microscopy) confirms the amyloid type fibril formation. UV–vis spectra, reported in Figure 6B, show the spectral shift of the conventional CR band from 488 to 540 nm after the addition of DOTA(Gd)-L_6-F4 in the couvette for two different concentrations (0.1 and 1.0 mg mL^{-1}). At the same time, air-dried films of gadolinium poly-phenylalanine derivatives stained with Congo Red and tetra-phenylalanine peptide dried fibers containing CR exhibit intense green birefringence when imaged with polarized optical microscopy (see Figure 6C and Figure S8, Supporting Information).

2.4. TEM and X-Ray Diffraction

The morphology of the self-assembled nanostructures was also assessed by TEM and X-ray diffraction. Selected images of DTPA(Gd)-L_6-F4 and DOTA(Gd)-L_6-F4 gadolinium complexes in water solution at 5.0 mg mL^{-1} show the presence of long nanofibers with a minimum thickness around 10 nm (**Figure 7**). The recorded XRD patterns from DOTA(Gd)-L_6-F4 and L_6-F4 peptide dried stalks are shown in **Figure 8**A,B, respectively.

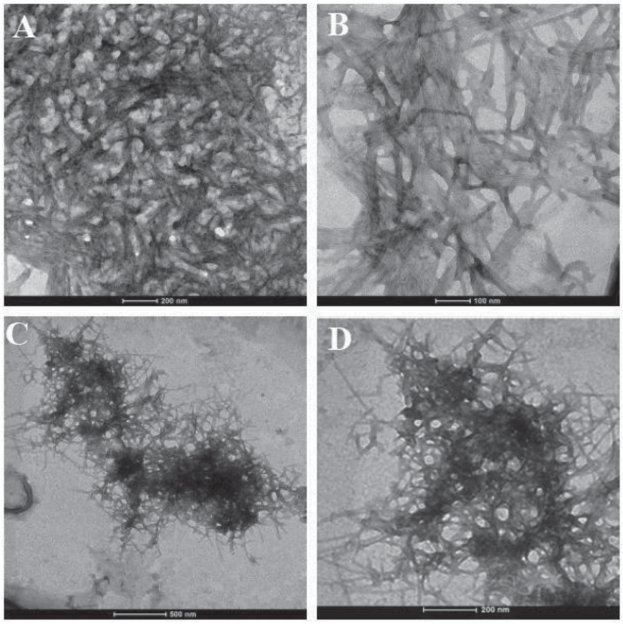

Figure 7. Selected TEM images for A,B) DOTA(Gd)-L_6-F4 at 5.0 mg mL^{-1} and C,D) DTPA(Gd)-L_6-F4 at 5.0 mg mL^{-1}. Scale bars are 200 nm for (A,D), 100 nm for (B), and 500 nm for (C).

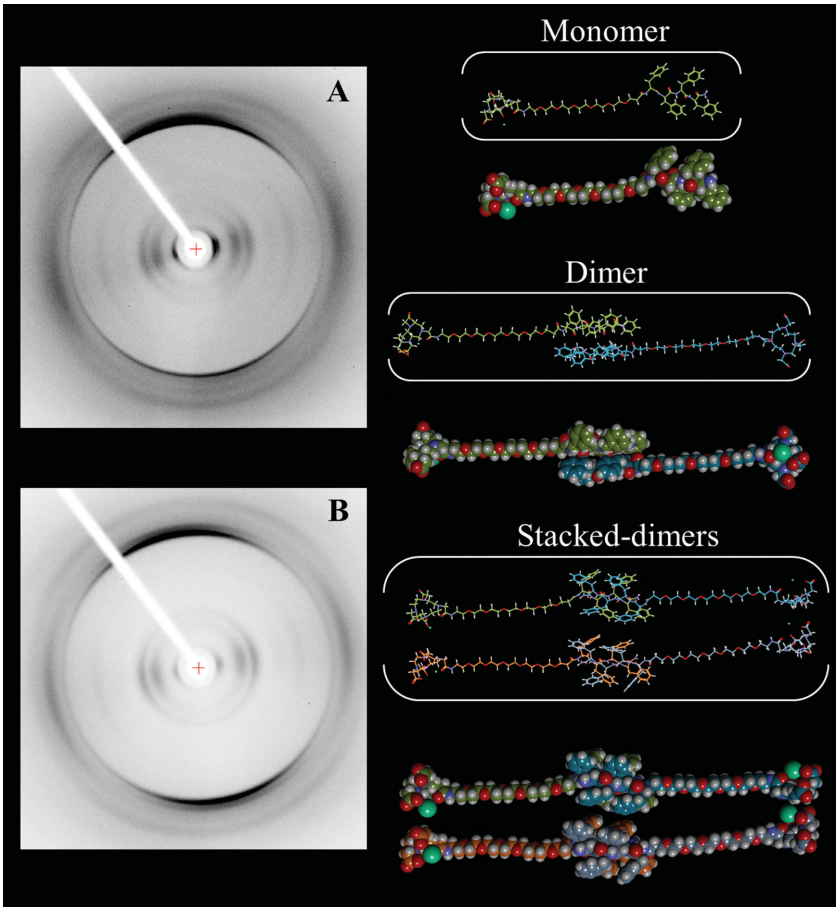

Figure 8. Selected X-ray fiber diffraction for A) DOTA-L_6-F4 and B) L_6-F4. The patterns show the diffraction features associated with the β-structure. Based on our experimental results, on the right side, a model of DOTA(Gd)-L_6-F4 as monomer, dimer and stacked-dimers is reported.

Miller indices and d-spacings for both fiber types were determined using the software *CLEARER* and are reported in Tables S1 and S2 of the Supporting Information. As clearly indicated from the diffraction pattern, the structural arrangement of the peghylated cationic tetra-phenylalanine was not significantly affected from the functionalization of the N-terminus with the DOTA (or DTPA, data not shown) chelating agents. Both the X-ray diffractions show the typical "cross-β" diffraction pattern of amyloid fibers, with a Bragg spacing of 4.8–4.9 Å along the meridian, generally attributed to the interchain distance between the hydrogen-bonded strands oriented perpendicularly to the fiber axis, and a more diffuse periodicity of ≈10 Å in the equatorial direction, usually ascribed to the staking of these β-sheets perpendicularly to the fiber axis.[39,40] These XRD results are in agreement with the above reported CD (Figure 5) and IR data (Figure 6A and Figure S6, Supporting Information) indicating a β-sheet conformation of DOTA(Gd)-L_6-F4 in a dried film. In Figure 8 it is also reported a simplified model in extended conformation of DOTA(Gd)-L_6-F4 based on our experimental results to better appreciate the monomer dimension (about 50 Å), the antiparallel two-stranded β-disposition of the dimer with the fiber axis pointing up the plane of the paper, and the stacked-dimers with the fiber axis pointing toward the observer.

2.5. Relaxometry

Gd-complexes are used as positive MRI contrast agents (CAs) as they are able to strongly enhance the water protons relaxation rate in aqueous solutions thanks to the magnetic dipolar interaction between unpaired electrons on the gadolinium ions and the water protons. Their efficacy as MRI CAs is thus measured on the basis of this ability, which is usually defined as longitudinal "relaxivity" (r_{1p}) and is referred to the water proton relaxation rate of a solution containing one millimolar concentration of the Gd-complex.

The relaxivity of a Gd-containing system depends on the complex interplay among structural, dynamic, and electronic parameters.[41] At the frequencies most commonly used in commercial tomographs (20–60 MHz), r_{1p} is generally determined by the reorientational correlation time (τ_R) of the chelate so that high molecular weight systems display higher relaxivity. Based on this property, it is possible to follow the occurrence of an aggregation process involving a Gd-complex through the measure of the water proton longitudinal relaxation rate of its aqueous solution. The relaxivities of DOTA(Gd)-L_6-F4 and DTPA(Gd)-L_6-F4, measured at 21.5 MHz (0.5 T) and 298 K as a function of the complex concentration, are reported in **Figure 9**A. The observed progressive enhancement in relaxivity is indicative of the self-aggregation of the two Gd-complexes. The inset in Figure 9A shows an amplification of the graph at low concentration values from which it is possible to observe that DTPA(Gd)-L_6-F4 starts to aggregate at higher concentrations than DOTA(Gd)-L_6-F4, reflecting the CAC values determined by fluorescence spectroscopy.

The analysis of the magnetic field dependence of the relaxivity, obtained through the registration of the so-called nuclear magnetic resonance dispersion (NMRD) profiles, allows the determination of the principal parameters characterising the relaxivity of a Gd(III) chelate. The NMRD profiles of DOTA(Gd)-L_6-F4 and DTPA(Gd)-L_6-F4, measured at 40 mg mL^{-1} concentration, are reported in Figure 9B. The shape of both the profiles, with the characteristic peak of relaxivity in the region of Proton Larmor Frequencies 10–70 MHz, is a clear indication that, at this concentration, the Gd-complexes are in an aggregated form. Data were fitted to the conventional Solomon–Bloembergen–Morgan theory[42,43] and the relative fitting parameters are reported in **Table 2**.

The high field relaxivity of the two complexes are quite similar, being, at 20 MHz, 14.8×10^{-3} and 14.0×10^{-3} $_M{}^{-1}$ s^{-1} for DOTA(Gd)-L_6-F4 and DTPA(Gd)-L_6-F4, respectively. The τ_R values found for the two complexes are in fact very close. On the other hand, the big difference in relaxivity observed in the low field region has to be ascribed to the difference in the electronic

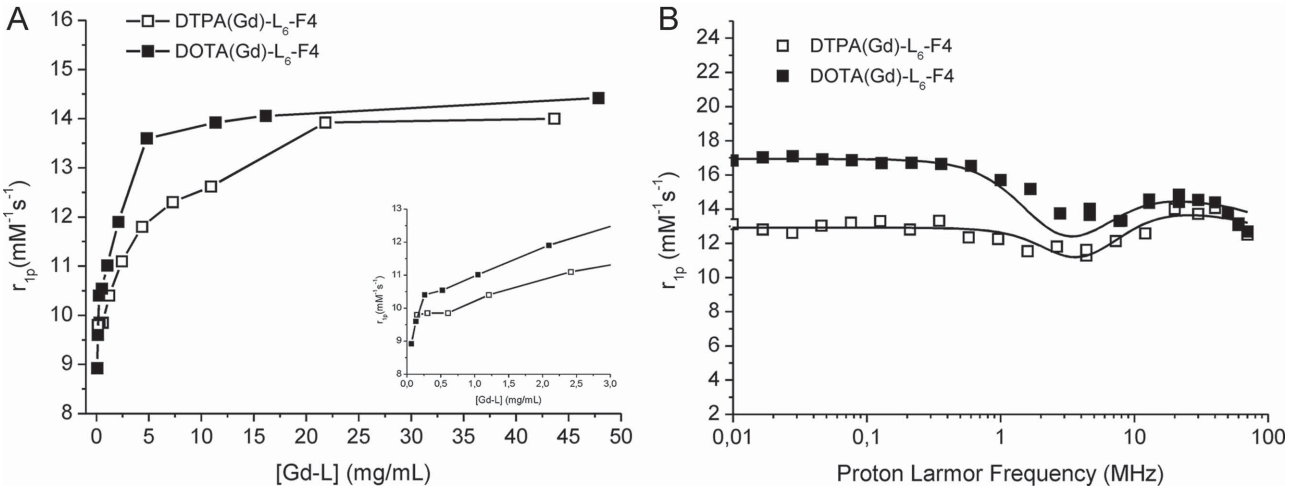

Figure 9. A) Longitudinal proton relaxivity of DOTA(Gd)-L_6-F4 and DTPA(Gd)-L_6-F4 measured at 21.5 MHz (0.5 T) and 298 K as a function of the concentration of the poly-phenylalanine Gd-complexes. B) Nuclear magnetic resonance dispersion (NMRD) profiles of the 40 mg mL^{-1} aqueous solutions of the two polyphenylalanine Gd-complexes at 298 K. The data refer to 1×10^{-3} M concentration of the paramagnetic complexes.

relaxation time (τ_{s0}) of the two Gd-complexes (Table 2). It is in fact known, that highly symmetric and rigid DOTA-type chelates generally have longer τ_{s0} values than DTPA-like, and this physically translates to a higher low-field relaxivity.[44] It is worth to note that the τ_R values extracted from the fitting procedure for DOTA(Gd)-L_6-F4 and DTPA(Gd)-L_6-F4 in the aggregated form are quite short if compared to those usually found for nanosized aggregates (1–30 ns). Likely, this finding can be explained with the occurrence of a quite fast internal motility of the Gd-complexes along the linker spacer with respect to the overall fibril-like structures, as evidenced in the model arrangement proposed in Figure 8.

2.6. Cytotoxicity and MRI Evaluation of the Cellular Uptake

The cytotoxicity of the fibril nanoaggregates of DOTA(Gd)-L_6-F4 and DTPA(Gd)-L_6-F4 has been initially tested in the mouse embryonic fibroblast cell line 3T3 in the concentration range 0.5–5.0 mg mL^{-1} (**Figure 10**A). With a view to the subsequent experiments on the evaluation of the MRI cellular response, given that the particles, in this preliminary stage, are not functionalized for a target-specific cellular internalization, it was necessary to push the uptake experiment with an overnight incubation. The cytotoxicity assay revealed a significant reduction in fibroblast viability along with the increase of the Gd-complexes concentration, with a higher effect in the case of DOTA(Gd)-L_6-F4 particles. The cytotoxicity appears to be higher than that reported in the case of analogous di-phenylalanine microtubes in the same cell line[21] because of the longer incubation time (overnight in our experiments vs 2 h in the literature data.[21]

A recent work on the assessment of the cellular response to dissolution and degradation products from self-assembled Fmoc-FF gels revealed that the critical factor affecting cell viability is the time a gel is allowed to degrade and leach into the media.[45] We taught that a way to elude a long incubation time while maintaining a sufficient amount of internalized probes to test their ability to enhance the MRI cellular response would be to use a macrophagic cell line which attitude is to phagocytize a huge amounts of particles in short times. Thus, the cytotoxicity of the fibril nanoaggregates of DOTA(Gd)-L_6-F4 and DTPA(Gd)-L_6-F4 was investigated in J774A.1 mouse macrophages (Figure 10B) in the same concentration range (0.5–5.0 mg mL^{-1}) but with an incubation time of 3 h. In this case, the treated cells showed the same viability of the control cells even at the higher concentrations. Next, the uptake efficiency of DOTA(Gd)-L_6-F4 and DTPA(Gd)-L_6-F4 nanoaggregates and their efficacy in enhancing the MR-signal upon internalization, were investigated in J774A.1 cells and compared to those of the parents Gd-DOTA (Dotarem, Guerbert

Table 2 Main relaxometric parameters derived from fitting of NMRD profiles at 21.5 MHz reported in Figure 10B.

System	r_{1p} [a)] [$\times 10^{-3}$ M^{-1} s^{-1}]	Δ^2 [b)] [s^{-2}]	τ_V [c)] [ps]	τ_{s0} [d)] [ps]	τ_R [e)] [ps]
DOTA(Gd)-L_6-F4	14.8	8.0×10^{18}	49	212	490
DTPA(Gd)-L_6-F4	14.0	1.25×10^{19}	52	127	457

[a)]On carrying out the fitting procedure, some parameters were fixed to reasonable values: r_{Gd-H} (distance between Gd and protons of the inner sphere water molecule) = 3.1 Å; a (distance of minimum approach of solvent water molecules to Gd^{3+} ion) = 3.8 Å; D (solvent diffusion coefficient) = 2.2×10^{-5} cm^2 s^{-1}; [b)]Squared mean transient zero-field splitting (ZFS) energy; [c)]Correlation time for the collision-related modulation of the ZFS Hamiltonian; [d)]Electronic relaxation time at zero field (calculated as $1/\tau_{s0} = 12\Delta^2 \times \tau_v$); [e)]Reorientational correlation time.

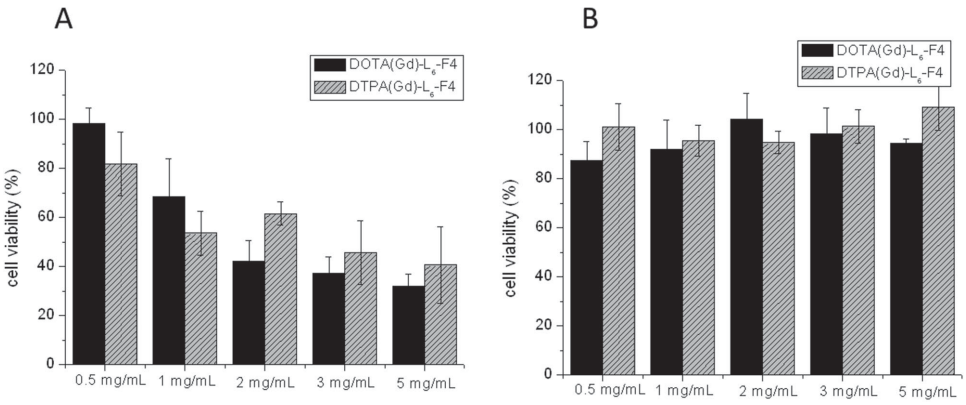

Figure 10. Cell viability percentage, evaluated by a CellTiter-Blue reagent test, after A) overnight treatment of the 3T3 fibroblasts and B) 3 h treatment of J774A.1 macrophages with various concentrations of DOTA(Gd)-L_6-F4 and DTPA(Gd)-L_6-F4. Data are expressed as the mean ± SD ($n = 3$).

SA, France) and Gd-DTPA (Magnevist, Schering AG, Germany) complexes. The cells were incubated with increasing concentrations of DOTA(Gd)-L_6-F4 and DTPA(Gd)-L_6-F4 for 3 h at 37 °C and the amount of internalized gadolinium determined through ICP-MS analysis (**Figure 11**A).

Both the tetraphenylalanine functionalized Gd-complexes, being under the form of aggregates, displayed internalization efficiency far higher than that of the control complexes. The cellular MRI-signal response to labelling with the Gd-complexes was investigated at 7.1 T (Figure 11B). The T_{1w} images of the cellular pellets, and the corresponding R_1 ($1/T_1$) values, reflect the trend of higher cellular internalization for F4-Gd complexes displayed in Figure 11A, being the signal intensity remarkably higher than that observed when J774A.1 cells were incubated with Gd-DOTA and Gd-DTPA. The comparison between the two F4-Gd complexes reveals a higher efficiency of DOTA(Gd)-L_6-F4 in enhancing the water proton MR-signal with respect to DTPA(Gd)-L_6-F4. The reason for this, likely, relies in the different aggregation state of the two Gd-complexes in the concentration used for this experiment. Both at 1.5×10^{-3} and 3.5×10^{-3} M^{-1} (corresponding to 2.0 and 5.0 mg mL^{-1}), in fact, as can be appreciated in Figure 9A, DOTA(Gd)-L_6-F4 is endowed with an higher relaxivity due to its higher aggregation tendency, while for DTPA(Gd)-L_6-F4 the relaxivity is lower. An accurate analysis of the observed relaxation rates of the pellets of cells, incubated with DOTA(Gd)-L_6-F4 and DTPA(Gd)-L_6-F4 with reference to the amount of internalized Gd-complexes, reveals that the increase in the uptake extent observed by passing from 1.5×10^{-3} to 3.5×10^{-3} M^{-1} concentration in the incubation media, is not accompanied by the corresponding enhancement in the relaxation rate (signal intensity) for each Gd-containing system. This behavior can be explained on the basis of the previously observed "quenching" effect on the relaxivity taking place when cells are labelled with high amounts of Gd-complexes and is related to the confinement of the probe in the sub-cellular or cellular compartments.[46,47] The MRI contrast effect is not limited by insufficient loading with paramagnetic material, but by the exchange rate of water molecules across the endosomal or cellular membrane.

3. Conclusions

The synthesis and the structural characterization of novel potential MRI contrast agents based on the aggregation of polyphenylalanine conjugates have been reported. The insertion of

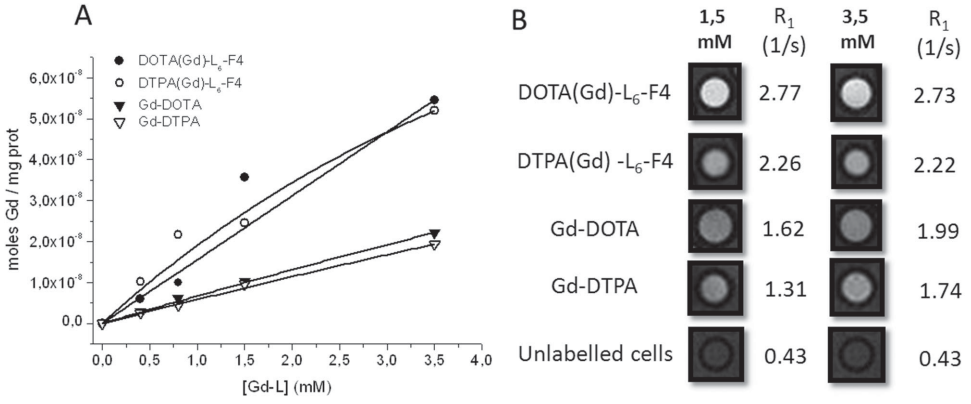

Figure 11. A) Amount of internalized gadolinium ions, evaluated by ICP-MS, in J774A.1 cells incubated with increasing concentrations of DOTA(Gd)-L_6-F4, DTPA(Gd)-L_6-F4, Gd-DOTA, and Gd-DTPA for 3 h. B) T_1-weighted MR-images, and relative observed relaxation rates, of pellets of J774A.1 cells labelled with 1.5 and 3.5×10^{-3} M DOTA(Gd)-L_6-F4, DTPA(Gd)-L_6-F4, Gd-DOTA, and Gd-DTPA.

a DTPA or a DOTA gadolinium complex on the N-terminus FF homodimer destroys both the head-to-tail interaction and the π–π intermolecular interaction of the aromatic framework. This effect can be probably attributed to the steric hindrance of the gadolinium complex. Hence, the peptide framework was reinforced by increasing the number of the phenylalanine residues from two to four. Both the DOTA and DTPA tetra-phenylalanine derivatives are able to self-aggregate at very low concentration, also after gadolinium coordination. Moreover, Gd(III) complexes are completely soluble in water, whereas a previously reported N-terminus-methoxy and C-terminus-ethyl protected F4-L_7 derivative showed a poor water solubility.[36] The structural characterization aimed to define the secondary structure of the peptide fragment confirms the amyloid type fibril formation in which, as expected, an antiparallel alignment is preferred. Amyloid type fibril formation was also confirmed by TEM images and X-ray diffraction patterns. Moreover, the self-aggregation of DOTA(Gd)-L_6-F4 and DTPA(Gd)-L_6-F4 has been proved by the progressive enhancement in relaxivity observed increasing the Gd complex concentration and by the typical shape of the NMRD profiles in the region of Proton Larmor Frequencies 10–70 MHz. The relaxivity values of the two complexes at 20 MHz are 14.8×10^{-3} and 14.0×10^{-3} $_M{}^{-1}$ s^{-1} for DOTA(Gd)-L_6-F4 and DTPA(Gd)-L_6-F4, respectively. These values are higher than the classical contrast agents at low molecular weight. On the other hand, these values are comparable or lower than many examples of Gd(III)-based micelle or liposome contrast agents.[23–30] Surprising the τ_R values extracted from the fitting procedure are quite short if compared to those usually found for nano-sized aggregates (1–30 ns). In our opinion, these low τ_R values can be attributed to the occurrence of a quite fast internal motility of the Gd-complexes along the linker spacer with respect to the overall fibril-like structures. Preliminary studies aimed to define the ability of DOTA(Gd)-L_6-F4 and DTPA(Gd)-L_6-F4 to enhance the MRI cellular response was achieved on J774A.1 mouse macrophages cell line in which the cytotoxicity of the fibril nanoaggregates was negligible with an incubation time of 3 h in 0.5–5.0 mg mL^{-1} concentration range. The in vitro MRI behavior of nanoaggregates was also compared to those of the parents Gd-DOTA and Gd-DTPA complexes. Both the tetra-phenylalanine Gd-complexes showed a significant internalization efficiency and a remarkably enhance of the water proton MR-signal with respect to the control complexes. Moreover, the higher efficiency of DOTA(Gd)-L_6-F4 in enhancing the water proton MR-signal with respect to DTPA(Gd)-L_6-F4 probably reflects the different aggregation state of the two Gd-complexes in the concentration used for this experiment. At the best of our knowledge, this is the first example of aromatic framework based nanoaggregates as MRI contrast agent. However, several issues have to improve before their in vivo applications as diagnostic tools. For example, the insertion of structural elements able to confer rigidity to the molecules without to alter their solubility could lead to higher relaxivity values. At the same time, synthetic modifications of the peptide framework, e.g., the replacement of natural amino acids with uncoded ones, could improve the stability of the fibrillary aggregates, thus reducing the extent of degradation products that are invocated as the critical factor affecting cell viability into the cellular media.

4. Materials and Methods

Protected Nα-Fmoc-amino acid derivatives, coupling reagents, and Rink amide MBHA (4-methylbenzhydrylamine) resin were purchased from Calbiochem-Novabiochem (Laufelfingen, Switzerland). The Fmoc-21-amino-4,7,10,13,16,19-hexaoxaheneicosanoic acid [Fmoc-Ahoh-OH, (L_6)] and the Fmoc-8-amino-3,6-dioxaoctanoic acid [Fmoc-AdOO-OH, (L_2)] were purchased from Neosystem (Strasbourg, France). DTPA(OtBu)$_4$-OH and DOTA(OtBu)$_3$-OH chelating agents were purchase from Chemateck (Dijon, France). All other chemicals were commercially available by Sigma-Aldrich (Milan, Italy) or Fluka (Bucks, Switzerland) or LabScan (Stillorgan, Dublin, Ireland) and were used as received unless otherwise stated. All solutions were prepared by weight with doubly distilled water. Preparative RP-HPLCs were carried out on a LC8 Shimadzu HPLC system (Shimadzu Corporation, Kyoto, Japan) equipped with an UV lambda-Max Model 481detector using Phenomenex (Torrance, CA) C18 column. Elution solvents are H_2O/0.1% TFA (A) and CH_3CN/0.1% TFA (B), from 5% to 70% over 30 min at 20 mL min^{-1} flow rate. Purity and identity of the products were assessed by analytical LC-MS analyses by using Finnigan Surveyor MSQ single quadrupole electrospray ionization (Finnigan/Thermo Electron Corporation San Jose, CA), column: C18-Phenomenex eluted with an H_2O/0.1% TFA (A) and CH_3CN/0.1% TFA (B) from 5% to 70% over 15 min at 200 µL min^{-1} flow rate.

Synthesis of Peptide Derivatives: Peptides and peptide conjugates were synthesized by using standard solid-phase 9-fluorenylmethoxycarbonyl (Fmoc) procedures. The Rink amide MBHA resin (substitution 0.65 mmol g^{-1}) was used as the solid phase support to provide the peptides as C-terminus amide, and synthesis was performed on a scale of 0.2 mmol. The resin was swelled in DMF for 30 min and the Fmoc deprotection reaction (10 min) was performed twice with 30% (v/v) piperidine in DMF. The amino acid coupling was achieved by adding twofold molar excess of amino acid, mixed with equimolar amounts of 1-hydroxybenzotriazole (HOBt), benzotriazol-1-yl-oxy-tris-pyrrolidino-phosphonium (PyBop), and fourfold molar excess of diisopropylethylamine (DIPEA) in DMF. All couplings were performed twice for 1 h. Chelating agents and the ethoxylic spacers (Fmoc-AdOO-OH and Fmoc-Ahoh-OH) were coupled as previously described.[48,49] Peptides were fully deprotected and from the resin with the TFA (trifluoroacetic acid)/ TIS (triisopropylsilane)/ H_2O (95.5/2.0/2.5 v/v/v) mixture at room temperature. Peptides and peptide conjugates were precipitated with ice-cold ethyl ether, dissolved in H_2O/CH_3CN and freeze-dried. The purification of the crude products was carried out by RP-HPLC. Mass spectra confirm the products identity. Retention times (R_t) and molecular weight (M_w) of the peptide derivatives are reported in **Table 3**.

DTPA-F2: ^{1}H-NMR (CD_3OD) (chemical shifts in δ, CH_3OH as internal standard 3.55) = 7.51-7.42 (m, 10 C*H* aromatic), 4.96-4.86 (m, 2H, C*H* Phe α), 4.65-4.61 (d, J = 16 Hz, 1H, R_2NCH_2CONHR), 4.44-4.40 (d, J = 16 Hz, 1H, R_2NCH_2CONHR), 3.87 (s, 8H, R_2NCH_2COOH), 3.53-3.50 (m, 4H, $R_2NCH_2CH_2NR_2$), 3.42-3.31 (m, 4H, $R_2NCH_2CH_2NR_2$), 3.24-2.99 (m, 4H, CH_2 Phe β).

Table 3. Retention time (R_t) and theoretical molecular weight (M_W) of investigated polyphenylalanine conjugates. RP-HPLC method and column details are reported in the Materials and Methods Section.

Sample	Formula	R_t [min]	M_W [u.m.a.]
DTPA-F2	$C_{32}H_{42}N_6O_{11}$	10.34	686
DOTA-F2	$C_{34}H_{46}N_6O_{10}$	10.65	698
DTPA-L_2-F2	$C_{38}H_{53}N_7O_{14}$	11.19	831
DOTA-L_2-F2	$C_{40}H_{57}N_7O_{13}$	11.42	843
DTPA-L_6-F2	$C_{47}H_{70}N_7O_{18}$	12.10	1020
DOTA-L_6-F2	$C_{49}H_{76}N_8O_{16}$	12.33	1032
L_6-F4	$C_{51}H_{67}N_6O_{11}$	15.30	939
DTPA-L_6-F4	$C_{65}H_{88}N_9O_{20}$	14.54	1314
DOTA-L_6-F4	$C_{67}H_{94}N_{10}O_{18}$	14.59	1326

DOTA-F2: ^{1}H-NMR (CD_3OD) (chemical shifts in δ, CH_3OH as internal standard 3.55) = 7.51-7.42 (m, 10 C*H* aromatic), 4.86-4.75 (m, 2H, C*H* Phe α), 3.70 (s, 6H, R_2NCH_2COOH), 3.45 (s, 16H, R_2N-$CH_2CH_2NR_2$), 3.40-3.36 (m, 2H, R_2NCH_2CONH), 3.16-2.90 (m, 4H, CH_2 Phe β).

DTPA-L_2-F2: ^{1}H-NMR (CD_3OD) (chemical shifts in δ, CH_3OH as internal standard 3.55) = 7.51-7.42 (m, 10 C*H* aromatic), 4.96-4.86 (m, 2H, C*H* Phe α), 4.55 (s, 2H, R_2NCH_2CONHR), 3.87 (s, 8H, R_2NCH_2COOH), 3.79 (s, 4H, OCH_2CH_2O), 3.75 (t, J = 4 Hz, 2H, $RNHCH_2CH_2O$), 3.65 (s, 2H, OCH_2COR), 3.60 (t, J = 7 Hz, 2H, $RNHCH_2CH_2O$), 3.53-3.50 (m, 4H, $R_2NCH_2CH_2N$ R_2), 3.42-3.31 (m, 4H, $R_2NCH_2CH_2NR_2$), 3.24-2.99 (m, 4H, CH_2 Phe β).

DOTA-L_2-F2: ^{1}H-NMR (CD_3OD) (chemical shifts in δ, CH_3OH as internal standard 3.55) = 7.51-7.42 (m, 10 C*H* aromatic), 4.86-4.75 (m, 2H, C*H* Phe α), 3.79 (s, 4H, OCH_2CH_2O), 3.75 (t, J = 4 *Hz*, 2H, RNH-CH_2CH_2O), 3.70 (s, 6H, R_2NCH_2COOH), 3.65 (s, 2H, OCH_2COR), 3.60 (t, J = 6 *Hz*, 2H, RNH-CH_2CH_2O), 3.45 (s, 16H, R_2N-$CH_2CH_2NR_2$), 3.40-3.36 (m, 2H, R_2NCH_2CONH), 3.16-2.90 (m, 4H, CH_2 Phe β).

DTPA-L_6-F2: ^{1}H-NMR (CD_3OD) (chemical shifts in δ, CH_3OH as internal standard 3.55) = 7.51-7.42 (m, 10 C*H* aromatic), 4.86-4.75 (m, 2H, C*H* Phe α), 4.55 (s, 2H, R_2NCH_2CONHR), 3.87 (s, 8H, R_2NCH_2COOH), 3.80 (s, 22H, OCH_2CH_2O), 3.75 (t, J = 8 Hz, 2H, $RNHCH_2CH_2O$), 3.68 (t, J = 7 Hz, 2H, $RNHCH_2CH_2O$), 3.40-3.32 (m, 6H, $R_2NCH_2CH_2NR_2$), 3.27-3.20 (dd, J = 7 Hz, J = 14 Hz, 2H, $R_2NCH_2CH_2NR_2$), 3.16-2.90 (m, 4H, CH_2 Phe β). 2.58 (t, J = 6 Hz, 2H, $NHCOCH_2CH_2$).

DOTA-L_6-F2: ^{1}H-NMR (CD_3OD) (chemical shifts in δ, CH_3OH as internal standard 3.55) = 7.51-7.42 (m, 10 C*H* aromatic), 4.86-4.75 (m, 2H, C*H* Phe α), 3.80 (s, 22H, OCH_2CH_2O), 3.75 (t, J = 4 *Hz*, 2H, $RNHCH_2CH_2O$), 3.70 (s, 6H, R_2NCH_2COOH), 3.60 (t, J = 6 *Hz*, 2H, $RNHCH_2CH_2O$, 3.45 (s, 16H, $R_2NCH_2CH_2NR_2$), 3.40-3.36 (m, 2H, R_2NCH_2CONH), 3.16-2.90 (m, 4H, CH_2 Phe β), 2.58 (t, J = 6 *Hz*, 2H, $NHCOCH_2CH_2O$).

L_6-F4: ^{1}H-NMR (CD_3OD) (chemical shifts in δ, CH_3OH as internal standard 3.55) = 7.51-7.42 (m, 20 C*H* aromatic), 4.86-4.75 (m, 4H, C*H* Phe α), 3.80 (s, 22H, OCH_2CH_2O), 3.75 (t, J = 4 *Hz*, 2H, $RNHCH_2CH_2O$), 3.60 (t, J = 6 *Hz*, 2H, $RNHCH_2CH_2O$), 3.16-2.90 (m, 8H, CH_2 Phe β), 2.58 (t, J = 6 *Hz*, 2H, $NHCOCH_2CH_2O$).

DTPA-L_6-F4: ^{1}H-NMR (CD_3OD) (chemical shifts in δ, CH_3OH as internal standard 3.55) = 7.51-7.42 (m, 20 C*H* aromatic), 4.86-4.75 (m, 4H, C*H* Phe α), 4.55 (s, 2H, R_2NCH_2CONHR), 3.87 (s, 8H, R_2NCH_2COOH), 3.80 (s, 22H, OCH_2CH_2O), 3.75 (t, J = 4 Hz, 2H, $RNHCH_2CH_2O$), 3.68 (t, J = 6 Hz, 2H, $RNHCH_2CH_2O$), 3.40-3.32 (m, 6H, $R_2NCH_2CH_2NR_2$), 3.27-3.20 (dd, J = 7 Hz, J = 14 Hz, 2H, $R_2NCH_2CH_2NR_2$), 3.16-2.90 (m, 8H, CH_2 Phe β), 2.58 (t, J = 6 *Hz*, 2H, $NHCOCH_2CH_2$).

DOTA-L_6-F4: ^{1}H-NMR (CD_3OD) (chemical shifts in δ, CH_3OH as internal standard 3.55) = 7.51-7.42 (m, 20 C*H* aromatic), 4.86-4.75 (m, 4H, C*H* Phe α), 3.80 (s, 22H, OCH_2CH_2O), 3.75 (t, J = 4 *Hz*, 2H, $RNHCH_2CH_2O$), 3.70 (s, 6H, R_2NCH_2COOH), 3.60 (t, J = 6 *Hz*, 2H, $RNHCH_2CH_2O$), 3.45 (s, 16H, $R_2NCH_2CH_2NR_2$), 3.40-3.36 (m, 2H, R_2NCH_2CONH), 3.16-2.90 (m, 8H, CH_2 Phe β), 2.58 (t, J = 6 *Hz*, 2H, $NHCOCH_2CH_2O$).

Preparation of Gadolinium Complexes: The complexation has been carried out by adding 1:1 molar ratio of $GdCl_3$ to the aqueous solutions of the DOTA or DTPA derivatives at neutral pH and room temperature. The amount of residual free Gd^{3+} ions was assessed by the orange xylenol UV method[50] and complexed by further addition of the corresponding amount of each ligand.

Fluorescence Studies: The values of critical aggregate concentration (CAC) were obtained by fluorescence measurements. Fluorescence spectra were recorded at room temperature on a Jasco Model FP-750 spectrofluorophotometer in a 1.0 cm path length quartz cell. Equal excitation and emission bandwidths (5 nm) were used throughout the experiments with a recording speed of 125 nm min^{-1} and automatic selection of the time constant. The CAC values were measured by using 8-anilino-1-naphthalene sulfonic acid ammonium salt (ANS)[51,52] and pyrene (Pyr) as fluorescent probes.[53]

Small aliquots of peptide conjugate in water solutions, as free bases or as gadolinium complexes, were added to 1.0 mL of aqueous solution of ANS (20×10^{-6} M) or Pyr (1×10^{-6} M). Final spectra, to be used for calculations, were obtained after blank correction and adjustment for dilution. The fluorescence intensity of ANS was followed as a function of the peptide concentration. The CAC values were determined by linear least-squares fitting of the fluorescence emission at 470 nm, upon excitation at 350 nm versus the polyphenylalanine concentration lower and higher than the change of slope. The excitation wavelength of Pyr was settled at 335 nm and spectra were recorded between 350 and 550 nm.

Thioflavin T (ThT) Spectroscopic Assay: Aggregation behavior of DOTA-L_6-F4 and DTPA-L_6-F4 as free bases or as gadolinium complexes was assessed by using Thioflavin T (ThT). Thioflavin T associates rapidly with β-aggregated peptides giving rise to an enhanced emission at 482 nm.[54] Fluorescence spectrum of an aqueous solution of ThT (25×10^{-6} M) before and after the addition of tetraphenylalanine derivatives (2 mg mL^{-1}) was recorded at 25 °C at regular intervals (each 10 min) during 2 h after the peptide addition into the cuvette. Samples were excited at 450 nm and fluorescence emission spectra were recorded between 460 and 650 nm.

Congo Red Spectroscopic Assay: UV–vis measurements of Congo Red (CR) alone or in presence of poly-phenylalanine

derivatives were carried out on Thermo Fisher Scientific Inc (Wilmington, Delaware, USA) Nanodrop 2000c spectrophotometer equipped with a 1.0 cm quartz cuvette (Hellma). A stock solution of CR (3.5 mg in 500 µL) was freshly prepared in 10×10^{-3} M phosphate buffer pH 7.4 and filtered through 0.2 µm syringe immediately prior to use. A small aliquot (5 µL) of this solution was diluted with the buffer at 12.5×10^{-6} M final concentration and the UV–vis spectrum was recorded between 400 and 700 nm at room temperature. 50 µL of DTPA(Gd)-L_6-F4 or DOTA(Gd)-L_6-F4 (20 mg mL^{-1}) were added to CR solution and samples were incubated for 30 min at room temperature. The spectra were recorded and background subtracted using a Congo Red spectrum in phosphate buffer as reference solution.

Circular Dichroism: Far-UV CD spectra of the peptide conjugates in aqueous solution were collected on a Jasco J-810 spectropolarimeter equipped with a NesLab RTE111 thermal controller unit using a 0.1 mm quartz cell at 25 °C. The spectra of samples at several concentrations (35, 20, 15, 10, 5, 2.0, 1.0, 0.5, and 0.1 mg mL^{-1}) are recorded from 280 to 195 nm. Other experimental settings were: scan speed, 10 nm min^{-1}; sensitivity, 50 mdeg; time constant, 16 s; bandwidth, 1 nm. Each spectrum was obtained by averaging three scans and corrected for the blank. Here Θ represents the mean residue ellipticity (MRE), i.e., the ellipticity per mole of peptide divided by the number of amino acid residues in the peptide. Thermal profiles (CD vs temperature, in the 10–80 °C range) of the tetraphenylalanine derivatives at 20 mg mL^{-1} were recorded every 10 °C, equilibrating for 10 min before next measurement.

Fourier Transform Infrared Spectroscopy (FTIR): FTIR spectra of samples (2.0 mg mL^{-1}) were collected on a Jasco FT/IR 4100 spectrometer (Easton, MD) in an attenuated total reflection (ATR) mode and using a Ge single-crystal at a resolution of 4 cm^{-1}. All the spectral data were processed using built-in software. Spectra were collected in transmission mode and then converted in emission. Each sample was recorded with a total of 100 scans with a rate of 2 mm s^{-1} against a KBr background.

Transmission Electron Microscopy (TEM) Images: TEM observation were performed with a transmission electron microscope FEI TECNAI G12 Spirit-Twin (LaB6 source) equipped with a bottom mounted FEI Eagle-4k CCD camera (Eindhoven, The Netherlands), operating with an acceleration voltage of 120 kV (LaMest Pozzuoli, Italy). A droplet of the sample solution (5 mg mL^{-1}) was placed onto a 400 mesh holey-carbon coated copper grid, air-dried for 1 h, and then negatively stained with phosphotungstic acid in water solution (1 wt%). Tomography holder with FEI Eagle 4K CCD camera and Xplore 3D software were used to obtain digital images.

X-ray Fiber Diffraction (XRD): Diffraction patterns were obtained for stalks prepared by the stretch frame method.[55] Briefly, a droplet (10 µL) of peptide aqueous solution (3 wt%) was suspended between the ends of a wax-coated capillary (spaced 2 mm apart). The droplet was allowed to dry gently at room temperatures overnight to obtain oriented fibers. The stalk was mounted vertically onto the four axis goniometer of an R-AXIS IV++ X-ray diffractometer (Rigaku) equipped with a rotating anode generator. The XRD data were collected using a Saturn 944 CCD camera (CuKα high intensity X-ray microfocus source, $\lambda = 1.5418$ Å). The specimen-to-film distance was set at 90 mm and the exposure time was set to 60 s. The X-ray patterns were processed using the analysis and simulation *CLEARER* software.[56]

Congo Red Staining and Polarized Optical Microscopy: Dried film of polyphenylalanine was obtained placing 10 µL of the peptide aqueous solution (3 wt%) onto a glass slide and left drying at room temperature. Then, the air-dried samples were stained with 150 µL of freshly prepared CR solution, obtained adding a saturating amount of CR in ethanol containing 20% of NaCl saturated water. After the application of the CR solution, the excess was rapidly removed from the glass slide with a filter paper. CR containing fibers were prepared, as above described with stretch frame method, adding 2 µL of CR staining solution to 50 µL of poly-phenylalanine solution. Samples dried on glass slide or CR containing fibers were observed under bright field illumination and between crossed polars using a Nikon AZ100 microscope.

Water Proton Relaxation Measurements: The longitudinal water proton relaxation rates were measured at 25 °C by using a Stelar Spinmaster (Stelar, Mede, Pavia, Italy) spectrometer operating at 0.5 T (21.5 MHz Proton Larmor Frequency), by mean of the standard inversion-recovery technique. The temperature was controlled with a Stelar VTC-91 air-flow heater equipped with a copper constantan thermocouple (uncertainty 0.1 °C). The proton $1/T_1$ NMRD profiles were measured at 25 °C on a fast field-cycling Stelar relaxometer over a continuum of magnetic field strengths from 0.00024 to 0.47 T (corresponding to 0.01–20 MHz proton Larmor frequencies). The relaxometer operates under computer control with an absolute uncertainty in $1/T_1$ of ±1%. Additional data points in the range 21.5–70 MHz were obtained on the Stelar Spinmaster spectrometer. The concentration of the solutions used for the relaxometric characterization was determined according to a previously reported relaxometric method.[57] Data were fitted to the conventional Solomon–Bloembergen–Morgan theory.

Cytotoxicity Studies: The cytotoxicity of DOTA(Gd)-L_6-F4 and DTPA(Gd)-L_6-F4 probes was investigated in a mouse macrophages cell line (J774A.1) and in a mouse embryonic fibroblast cell line (3T3). J774A.1 and 3T3 cells were seeded in DMEM culture medium, enriched with 10% fetal bovine serum and 1% glutamine, at 150 000 and 50 000 cells per well, respectively, in 96-well plates the day before the incubation. The cells were incubated for 3 h (J774A.1) or overnight (3T3) at 37 °C with the two Gd-based probes at different concentrations: 0.5, 1, 2, 3, and 5 mg mL^{-1}. After the incubation, cells were gently washed and re-incubated for 4 h with 20 µL of CellTiter-Blue reagent for the viability test. The CellTiter-Blue reagent is a solution containing resazurin, an indicator dye, which has little intrinsic fluorescence with the maximum absorbance at 605 nm. The reagent undergoes a "blue shift" upon reduction of resazurin to resorufin with a maximum peak at 573 nm. The fluorescence produced is proportional to the number of viable cells. The same amount of CellTiter-Blue reagent was added to triplicate wells without cells (no-cell control) and with untreated cells (control cells), respectively. At the end of the incubation, the fluorescence at 560/590 nm was measured using the fluorometric method. The experiments were carried out in triplicate. Obtained data were analysed subtracting the mean fluorescence value of the culture background from all fluorescence values of

experimental wells. The percentage of viable cells was calculated according to the following equation:

$$\% \text{ viable cell} = \frac{\text{experimental cells mean value}}{\text{control cells mean value}} \times 100 \quad (1)$$

Cellular Uptake Studies: Approximately 1×10^6 J774A.1 cells, in DMEM medium, were incubated with different concentrations of DOTA(Gd)-L_6-F4 and DTPA(Gd)-L_6-F4 for 3 h at 37 °C. After this incubation time, the cells were washed three times with 5 mL ice-cold phosphate-buffered saline (PBS), detached with a scraper and, for the acquisition of the MR images, collected in 50 µL of PBS, transferred into glass capillaries that were centrifuged at 1500 rpm for 5 min and placed in an agar phantom. The MR images were acquired by standard T_1-weighted spin-echo sequence (TE = 2.6 ms, 16 variable TR ranging from 50 to 8000 ms, NEX = 1, FOV = 1.1 × 1.1 cm^2, 1 slice, slice thickness = 1 mm) and recorded on a Bruker Avance300 operating at 7 T. After imaging, the labeled cells were suspended in 200 µL PBS and sonicated to obtain cell lysates. Gd(III) content was measured by ICP-MS analysis (Element-2; Thermo-Finnigan, Rodano Milan, Italy). The preparation of the samples for ICP-MS analysis has been carried out as follows: i) 150 µL of each cell lysate was mineralized with 1 mL of concentrated HNO_3 (65% v/v) under microwave heating at 160 °C for 40 min (Milestone MicroSYNTH Microwave lab station equipped with an optical fiber temperature control and HPR-1000/6M six position high-pressure reactor, Bergamo, Italy); ii) after mineralization, the volume of each sample was brought to 2 mL with ultrapure water and the sample was analyzed by ICP-MS. The calibration curve was obtained using four gadolinium absorption standard solutions (Sigma-Aldrich) in the range 0.005–0.2 µg mL^{-1}. The protein content of cells lysates was determined by the Bradford method using bovine serum albumin as standard.

Supporting Information

Supporting Information is available from the Wiley Online Library or from the author.

Acknowledgements

The authors are indebted with the Italian Minister for Research (M.I.U.R.) for financial support under FIRB "RENAME" RBAP114AMK and PRIN 2012SK7ASN projects. The authors thank Mr. Leopoldo Zona and Giosuè Sorrentino for technical support.

Received: June 16, 2015
Revised: September 17, 2015
Published online: October 21, 2015

[1] S. I. Stupp, *Nano Lett.* **2010**, *10*, 4783.
[2] S. Cavalli, F. Albericio, A. Kros, *Chem. Soc. Rev.* **2010**, *39*, 241.
[3] K. Morris, L. Serpell, *Chem. Soc. Rev.* **2010**, *39*, 3445.
[4] S. J. Rymer, S. J. B Tendler, C. Bosquillon, C. Washington, C. J. Roberts, *Ther. Delivery* **2011**, *2*, 1043.
[5] H. Cui, M. J. Webber, S. I. Stupp, *Biopolymers* **2010**, *94*, 1.
[6] S. Fleming, R. V. Ulijn, *Chem. Soc. Rev.* **2014**, *43*, 8150.
[7] I. W. Hamley, *Angew. Chem. Int. Ed.* **2014**, *53*, 6866.
[8] T. P. Carberry, R. Tarallo, A. Falanga, E. Finamore, M. Galdiero, M. Weck, S. Galdiero, *Chem. Eur. J.* **2012**, *18*, 13678.
[9] D. Tesauro, A. Accardo, E. Gianolio, L. Paduano, J. Teixeira, K. Schillen, S. Aime, G. Morelli, *ChemBioChem* **2007**, *8*, 950.
[10] A. Accardo, D. Tesauro, G. Mangiapia, C. Pedone, G. Morelli, *Biopolymers* **2007**, *88*, 115.
[11] T. Ji, Y. Ding, Y. Zhao, J. Wang, H. Qin, X. Liu, J. Lang, R. Zhao, Y. Zhang, J. Shi, N. Tao, Z. Qin, G. Nie, *Adv. Mater.* **2015**, *27*, 1865.
[12] M. Reches, E. Gazit, *Science* **2003**, *300*, 625.
[13] X. Yan, P. Zhu, J. Li, *Chem. Soc. Rev.* **2010**, *39*, 1877.
[14] I. Azuri, L. Adler-Abramovich, E. Gazit, O. Hod, L. Kronik, *J. Am. Chem. Soc.* **2014**, *136*, 963.
[15] P. Tamamis, L. Adler-Abramovich, M. Reches, K. Marshall, P. Sikorski, L. Serpell, E. Gazit, G. Archontis, *Biophys. J.* **2009**, *96*, 5020.
[16] C. Guo, Y. Luo, R. Zhou, G. Wei, *ACS Nano* **2012**, *6*, 3907.
[17] R. Huang, W. Qi, L. Feng, R. Su, Z. He, *Soft Matter* **2011**, *7*, 6222.
[18] N. Gour, D. Kedracki, I. Safir, K. X. Ngo, C. Vebert-Nardin, *Chem. Commun.* **2012**, *48*, 5440.
[19] M. I. Souza, Y. M. Jaques, G. P. de Andrade, A. O. Ribeiro, E. R. da Silva, E. E. Fileti, É. d. S. Ávilla, M. V. B. Pinheiro, K. Krambrock, W. A. Alves, *J. Phys. Chem. B* **2013**, *117*, 2605.
[20] T. O. Mason, D. Y. Chirgadze, A. Levin, L. Adler-Abramovich, E. Gazit, T. P. J. Knowles, A. K. Buell, *ACS Nano* **2014**, *8*, 1243.
[21] R. F. Silva, D. R. Araújo, E. R. Silva, R. A. Ando, W. A. Alves, *Langmuir* **2013**, *29*, 10205.
[22] H. Zang, J. Fei, X. Yan, A. Wang, J. Li, *Adv. Funct. Mater.* **2015**, *25*, 1193.
[23] A. Accardo, D. Tesauro, G. Morelli, E. Gianolio, S. Aime, M. Vaccaro, G. Mangiapia, L. Paduano, K. Schillén, *J. Biol. Inorg. Chem.* **2007**, *12*, 267.
[24] S. Torres, M. I. M. Prata, A. C. Santos, J. P. Andre, J. A. Martins, L. Helm, E. Toth, M. L. Garcia-Martin, T. B. Rodrigues, P. Lopez-Larrubia, S. Cerdán, C. F. G. C. Geraldes, *NMR Biomed.* **2008**, *21*, 322.
[25] E. Torres, F. Mainini, R. Napolitano, F. Fedeli, R. Cavalli, S. Aime, E. Terreno, *J. Controlled Release* **2011**, *154*, 196.
[26] M. Vaccaro, G. Mangiapia, L. Paduano, E. Gianolio, A. Accardo, D. Tesauro, G. Morelli, *ChemPhysChem* **2007**, *8*, 2526.
[27] A. T. Preslar, G. Parigi, M. T. McClendon, S. S. Sefick, T. J. Moyer, C. R. Haney, E. A. Waters, K. W. MacRenaris, C. Luchinat, S. I. Stupp, T. J. Meade, *ACS Nano* **2014**, *8*, 7325.
[28] S. R. Bull, M. O. Guler, R. E. Bras, T. J. Meade, S. I. Stupp, *Nano Lett.* **2005**, *5*, 1.
[29] S. Aime, D. Delli Castelli, S. Geninatti Crich, E. Gianolio, E. Terreno, *Acc. Chem. Res.* **2009**, *42*, 822.
[30] A. Accardo, D. Tesauro, L. Aloj, C. Pedone, G. Morelli, *Coord. Chem. Rev.* **2009**, *253*, 2193.
[31] V. Castelletto, I. W. Hamley, *Biophys. Chem.* **2009**, *141*, 169.
[32] M. R. Nilsson, *Methods* **2004**, *34*, 151.
[33] A. Morisco, A. Accardo, E. Gianolio, D. Tesauro, E. Benedetti, G. Morelli, *J. Pept. Sci.* **2009**, *15*, 242.
[34] N. Tzokova, C. M. Fernyhough, M. F. Butler, S. P. Armes, A. J. Ryan, P. D. Topham, D. J. Adams, *Langmuir* **2009**, *25*, 11082.
[35] R. Huang, R. Su, W. Qi, J. Zhao, Z. He, *Nanotechnology* **2011**, *22*, 245609.
[36] N. Tzokova, C. M. Fernyhough, P. D. Topham, N. Sandon, D. J. Adams, M. F. Butler, S. P. Armes, A. J. Ryan, *Langmuir* **2009**, *25*, 2479.
[37] S. D. Moran, M. T. Zanni, *J. Phys. Chem. Lett.* **2014**, *5*, 1984.
[38] H. A. Behanna, J. J. J. M. Donners, A. C. Gordon, S. I. Stupp, *J. Am. Chem. Soc.* **2005**, *127*, 1193.
[39] L. C. Serpell, *Biochim. Biophys. Acta, Mol. Basis Dis.* **2000**, *1502*, 16.

[40] R. Orbach, I. Mironi-Harpaz, L. Adler-Abramovich, E. Mossou, E. P. Mitchell, V. T. Forsyth, E. Gazit, D. Seliktar, *Langmuir* **2012**, *28*, 2015.
[41] S. Aime, S. Geninatti Crich, E. Gianolio, G. B. Giovenzana, L. Tei, E. Terreno, *Coord. Chem. Rev.* **2006**, *250*, 1562.
[42] N. Blombergen, *J. Chem. Phys.* **1957**, *27*, 572.
[43] I. Solomon, *Phys. Rev.* **1955**, *99*, 559.
[44] P. Caravan, J. J. Ellison, T. J. McMurry, R. B. Lauffer, *Chem. Rev.* **1999**, *99*, 2293.
[45] W. T. Truong, Y. Su, D. Gloria, F. Braet, P. Thordarson, *Biomater. Sci.* **2015**, *3*, 298.
[46] E. Gianolio, F. Arena, G. J. Strijkers, K. Nicolay, A. Högset, S. Aime, *Magn. Reson. Med.* **2011**, *65*, 212.
[47] E. Di Gregorio, G. Ferrauto, E. Gianolio, S. Aime, *Contrast Media Mol. Imaging* **2013**, *8*, 475.
[48] A. Accardo, A. Morisco, E. Gianolio, D. Tesauro, G. Mangiapia, A. Radulescu, A. Brandt, G. Morelli, *J. Pept. Sci.* **2011**, *17*, 154.
[49] A. Accardo, P. Ringhieri, R. Palumbo, G. Morelli, *Biopolymers* **2014**, *102*, 304.
[50] A. Barge, G. Cravotto, E. Gianolio, F. Fedeli, *Contrast Media Mol. Imaging* **2006**, *1*, 184.
[51] K. S. Birdi, H. N. Singh, S. U. Dalsager, *J. Phys. Chem.* **1979**, *83*, 2733.
[52] E. De Vendittis, G. Palumbo, G. Parlato, V. Bocchini, *Anal. Biochem.* **1981**, *115*, 278.
[53] A. Nakajima, *J. Lumin.* **1976**, *11*, 429.
[54] H. LeVine III, *Protein Sci.* **1993**, *2*, 404.
[55] M. Sunde, L. C. Serpell, M. Bartlam, P. E. Fraser, M. B. Pepys, C. C. F. Blake, *J. Mol. Biol.* **1997**, *273*, 729.
[56] S. O. Makin, P. Sikorski, L. C. Serpell, *J. Appl. Cryst.* **2007**, *40*, 966.
[57] F. Arena, J. B. Singh, E. Gianolio, R. Stefanìa, S. Aime, *Bioconj. Chem.* **2011**, *22*, 2625.